

Investigation of anodic silicon dioxide thin films for microelectromechanical systems applications

Akarapu Ashok, Prem Pal

MEMS and Micro/Nano Systems Laboratory, Department of Physics, Indian Institute of Technology, Hyderabad, India
E-mail: ph11p1001@iith.ac.in

Published in Micro & Nano Letters; Received on 23rd June 2014; Revised on 10th September 2014; Accepted on 29th September 2014

In this reported work, silicon dioxide (SiO_2) thin films have been developed at room temperature using anodic oxidation of silicon. The effect of various process parameters on oxide properties including thickness, surface morphology, roughness and so on are investigated to determine the optimal conditions for the growth of SiO_2 for applications in microelectromechanical systems (MEMS). A spectroscopic ellipsometry was used to characterise the refractive index and thickness of the as-deposited films. Atomic force microscopy was employed to measure the surface roughness of the oxide films. To fabricate the overhanging micromechanical structures, the etch rate of the as-grown oxide film was studied in 25 wt% tetramethylammonium hydroxide and 10 wt% potassium hydroxide solutions at different temperatures. Finally, the as-grown oxide film is demonstrated for the fabrication of differently shaped MEMS components using an etchant showing minimum oxide etch rate.

1. Introduction: Silicon dioxide (SiO_2) thin films are extensively used in the fabrication of silicon-based integrated circuits and microelectromechanical systems (MEMS) for different purposes. In MEMS, it is primarily used as an etch mask, and as structural and sacrificial layers. SiO_2 is a very useful structural material for the development of freestanding microstructures (e.g. the cantilever beam) for the realisation of high-sensitivity sensors and actuators as it has a low elastic modulus in comparison to silicon and silicon nitride [1]. Among several thin film deposition methods such as thermal oxidation [2], anodic oxidation [3], chemical vapour deposition [4], sputtering [5] and so on, the anodic oxidation of silicon offers several advantages; for instance, it is very economic because of the simple equipment setup, it has easy handling and control over the oxide growth, and there is no involvement of toxic and expensive gases and so on.

In this Letter, SiO_2 thin films are synthesised at room temperature using the anodic oxidation method. The effect of different experimental parameters is studied. To exploit anodically grown oxide for MEMS using silicon wet anisotropic etching, the etch rates of as-grown oxide films were investigated in 25 wt% tetramethylammonium hydroxide (TMAH) and 10 wt% potassium hydroxide (KOH) at different temperatures. An etchant exhibiting a low oxide etch rate was utilised to fabricate different kinds of suspended structures (e.g. the rectangular cantilever beam, diaphragm etc.) and the cavities in {100} silicon substrate.

2. Experimental details: Czochralski (Cz) grown four-inch diameter P-type boron-doped (resistivity 1–10 $\Omega\text{-cm}$){100}-oriented single side polished silicon wafers were diced into a $23 \times 23 \text{ mm}^2$ chip size. The chips were cleaned ultrasonically in acetone for 5 min followed by thorough rinsing in deionised (DI) water. Aluminium was deposited on the rough surface side using DC sputtering for ohmic contact purpose. Ethylene glycol solvent (purity >99%, Merck) added with 0.04 M potassium nitrate (KNO_3) and different amounts of water was used as the electrolyte solution for oxide deposition. The pH of the solution was maintained at 4. Anodic oxidation was performed using a two-electrode system consisting of working and counter electrodes. The counter electrode can be of any convenient material, but it is usually chosen such that it should not produce chemical products by electrolysis that may potentially cause interfering reactions at the working electrode's surface. A

customarily designed sample holder that provides ohmic contact on the backside of the silicon sample was fixed as the anode (working electrode) and the platinum gauge mesh (90% platinum and 10% iridium) was used as the cathode (counter electrode). In all the experiments, the distance separating the electrodes was fixed at 1.5 cm. To etch out the native oxide prior to oxide growth, the sample was dipped in 1% hydrofluoric acid (HF) solution until it became hydrophobic, this step was followed by thorough rinsing in DI water. In the potentiodynamic mode of oxide synthesis, oxide growth was carried out at a fixed current density until the final voltage rose to the predetermined voltage of 300 V. Thereafter, the process was continued in potentiostatic mode at 300 V for 15 min. To investigate the effect of water content and current density on oxide properties, deposition was performed at different current densities (5.5, 8 and 10.5 mA/cm^2) in various amounts of water- (2.7, 4.7 and 6.7 vol%) added electrolytes. After the oxidation process, the oxidised samples were thoroughly cleaned in DI water to get rid of the adsorbed glycol solvent from the oxide surface. UV photolithography (Midas Mask Aligner, MDA 400 M) was employed for the patterning of the oxide layer. For the fabrication of differently shaped SiO_2 suspended microstructures and various size cavities on the Si{100} substrate, oxide etch rates were investigated in 25 wt% TMAH and 10 wt% KOH solutions. All etching experiments were carried out in a Teflon container equipped with a reflux condenser to prevent evaporation of the solution (or to avoid concentration change) during the etching process. Various characterisation techniques such as ellipsometry (J.A. Woolam, model: M-2000D), scanning electron microscopy (Zeiss, model: SUPRA40), optical microscopy (Olympus, STM6), a three-dimensional (3D) measuring laser microscope (Olympus, OLS4000), Fourier transform infrared (FTIR) spectroscopy (Bruker, model: TENSOR 37) and atomic force microscopy (Veeco, Multimode 8 with a ScanAsyst microscope) were employed for studying different characteristics of the as-grown oxide films and fabricated suspended microstructures.

3. Results and discussion

3.1. Growth characteristics: To study the effect of current density and electrolyte composition on oxide growth rate, the deposition was performed with varying current densities and the amounts of water added in the electrolyte. The variation in cell voltage during the

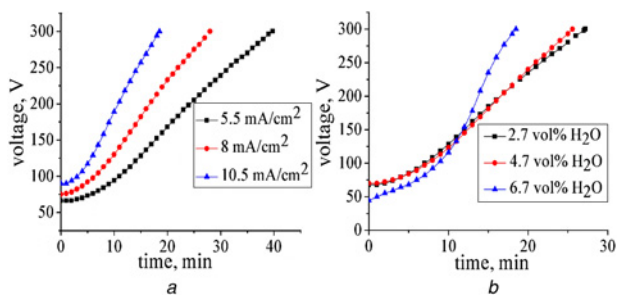


Figure 1 Variation in cell voltage with time
a At different current densities in 2.7 vol% water-added electrolyte
b For different amounts of water-added electrolytes at 8 mA/cm²

oxidation process was recorded for every minute and a graph plotted between the cell voltage and anodisation time, shown in Fig. 1. The curves in Fig. 1*a* represent the growth behaviour of oxide at 5.5, 8 and 10.5 mA/cm² current densities in 2.7 vol% water-added electrolyte. It can be observed from the graph that the voltage at the fixed applied current density increases continuously with time to maintain the constant current until the final voltage reaches the predetermined voltage of 300 V, which is primarily because of the increase in oxide thickness with time. The dependence of oxide growth rate on current density can also be explained from Fig. 1*a*, for instance, the time required to attain the predetermined voltage (i.e. 300 V) at 10.5 mA/cm² is shorter than the time needed at 5.5 and 8 mA/cm². Moreover, the rise in the slope with increasing current densities manifests the faster growth rate, which is attributed to the enhanced diffusion rate of oxygenic ions [6].

The curves in Fig. 1*b* show the growth characteristics of the oxides developed at 8 mA/cm² with varying water concentrations (2.7, 4.7 and 6.7 vol%) in the electrolyte. It can be noticed that with increasing water concentration the slope of the curves increases and the time required to attain the predetermined voltage (300 V) decreases, implying the dependency of oxide growth rate on water concentration. The enhanced growth rate at greater water concentrations may be because of the large concentration of oxygen and/or the high porosity of the film at the initial stage which allows faster diffusion of OH⁻ ions and/or oxygen in the film, thus leading to an improved growth rate in the later stage of oxidation [7, 8].

3.2. Ellipsometric characterisation: Ellipsometry is a non-destructive technique and widely used for thin film characterisation. It is employed to measure the thickness and refractive index of as-grown oxide films.

3.3. Thickness: The thicknesses of the as-grown oxide films were measured with varying angles of incidence (65°, 70° and 75°). The thicknesses of the oxides developed in 2.7 vol% water-added electrolyte at different current densities were measured to be from 155 to 156 nm. Analysis of the film thickness uniformity was performed by measuring the oxide thickness at four different locations as shown in Fig. 2 for the films grown at various current densities in an electrolyte comprising 2.7 vol% water concentration. It can be easily noticed that the film thickness is almost the same at different locations, indicating high thickness uniformity. Furthermore, it can be observed that the thickness does not vary with current density, implying that the ultimate thickness is controlled by the final voltage (i.e. 300 V).

Fig. 3 shows the thickness of the oxides developed at 8 mA/cm² in the electrolytes with varying water concentrations. In this Figure, it can be observed that the thickness is marginally affected by the water concentration.

3.4. Refractive index (RI): The RI of the as-grown oxide films deposited under different conditions were measured at 632.8 nm

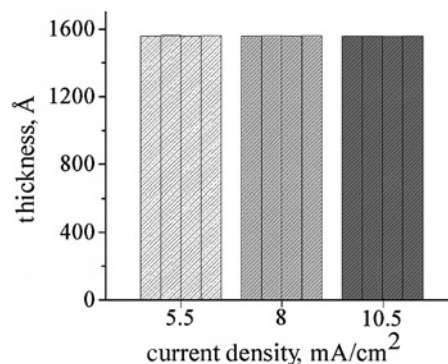


Figure 2 Comparison of film thicknesses measured at four different spots for the oxides deposited at different current densities in 2.7 vol% water-added electrolyte

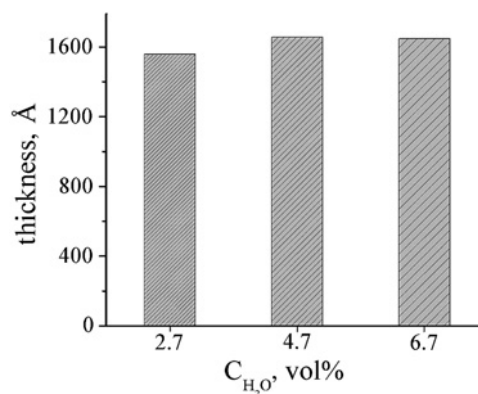


Figure 3 Dependence of oxide thickness on the amount of water in the electrolyte, at 8 mA/cm²

and are presented in Table 1. The RI of the oxide depends on its stoichiometry and density [9, 10]. It can be noticed from Table 1 that the RI decreases with an increase in the water concentration of the electrolyte. The RI of the oxides developed in 2.7 vol% water-added electrolyte at different current densities ranges from 1.474 to 1.475, which is slightly more than the refractive index of thermal oxide (1.462) [11]. The high RI is presumably because of the oxygen deficiency or the increase in film packing density [9, 10, 12]. The refractive index decreases for the films deposited in 4.7 and 6.7 vol% water-added electrolytes. This is because of the decrease in density or increase in the porosity of the film as the water content in the electrolyte increases [9, 10, 13].

3.5. FTIR analysis: FTIR was employed to determine the nature of the chemical bonds and the composition of the as-grown oxide films. The IR spectra of different samples oxidised up to the same final voltage (300 V) was recorded for 16 scans using the

Table 1 Refractive index of the as-grown oxides developed at different conditions, measured at a wavelength of 632.8 nm

Regime: Potentiodynamic; pH = 4		
Current density, mA/cm ²	Water content, vol%	Refractive index (<i>n</i>)
5.5	2.7	1.475
10.5	2.7	1.474
8	2.7	1.474
8	4.7	1.44
8	6.7	1.437

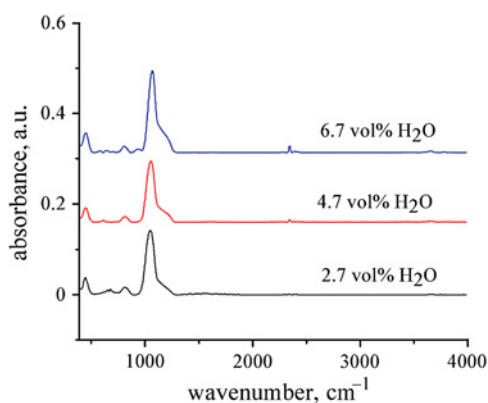


Figure 4 FTIR spectra of the oxide films deposited at 8 mA/cm^2 in the electrolytes containing different amounts of water

Bruker Tensor 37 in the wave number range $400\text{--}4000 \text{ cm}^{-1}$ (resolution 4 cm^{-1}). Fig. 4 shows the comparison of the IR absorption spectra of the oxides grown in the electrolyte containing different amounts of water at 8 mA/cm^2 . SiO_2 exhibits three characteristic vibrational modes, namely rocking ($445\text{--}450 \text{ cm}^{-1}$), bending ($800\text{--}815 \text{ cm}^{-1}$) and asymmetric stretching mode (ASM) ($1040\text{--}1080 \text{ cm}^{-1}$) [14, 15].

In Fig. 4, the characteristic vibrational modes of the as-grown anodic oxide films observed are rocking ($446\text{--}453 \text{ cm}^{-1}$), bending ($807\text{--}815 \text{ cm}^{-1}$), ASM ($1049\text{--}1069 \text{ cm}^{-1}$) and there is a weak shoulder characteristic of SiO_2 at about 1200 cm^{-1} [14, 15]. It can be seen from Fig. 4 that the peak corresponding to the ASM mode in the as-grown oxide films is obtained at a lower frequency as compared with 1080 cm^{-1} of the thermally grown SiO_2 film [9, 10]. The shifting of the ASM peak to a lower frequency is attributed to either oxygen deficiency or a smaller Si–O–Si bond angle because of the compressive stress generated in the films during oxide growth [9, 10, 16, 17]. However, the ASM peak shifts to a higher frequency (i.e. $1049\text{--}1069 \text{ cm}^{-1}$) as the water content in the electrolyte increased from 2.7 to 6.7 vol%. This could be because of the increased oxygen concentration or change in the Si–O–Si bond angle [9, 18]. Further examination of the spectra of the sample deposited in 6.7 vol% water-added electrolyte reveals two weak intense peaks at 940 and 3650 cm^{-1} corresponding to Si–OH vibrations [14, 15]. Therefore, the increase in water content causes the incorporation of hydroxyl ions in the film. Furthermore, the increase in the intensity of the broad shoulder at about 1200 cm^{-1} together with the presence of peak at 3650 cm^{-1} reflects the presence of porosity in the film with increasing water concentration in the electrolyte [19, 20].

3.6. Surface morphology study: To investigate the effect of different parameters on the oxide surface morphology, the oxidised samples were characterised using a scanning electron microscope (SEM).

The SEM micrographs of the oxide films deposited in 2.7 vol% water-added electrolyte at 5.5 and 8 mA/cm^2 current densities are presented in Figs. 5a and b, respectively. It can be realised from the SEM micrographs that the films are smooth, uniform and dense. The surface morphologies of the oxide films developed at 8 mA/cm^2 in 4.7 and 6.7 vol% water-added electrolytes are shown in Figs. 6a and b, respectively. In both cases, the unevenness in the surface can be easily noticed. This uneven surface may be because of the localised thickening of the oxide [21].

3.7. AFM analysis: The surface roughness of the as-deposited films was measured using AFM. The 2D AFM micrographs of the films deposited at 8 mA/cm^2 in 2.7 and 6.7 vol% water-added electrolytes are presented in Figs. 7a and b, respectively. It can

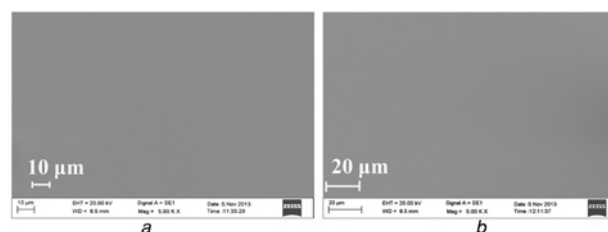


Figure 5 SEM micrographs of the oxide films developed in 2.7 vol% H_2O -added electrolyte at 5.5 and 8 mA/cm^2
a 5.5 mA/cm^2
b 8 mA/cm^2

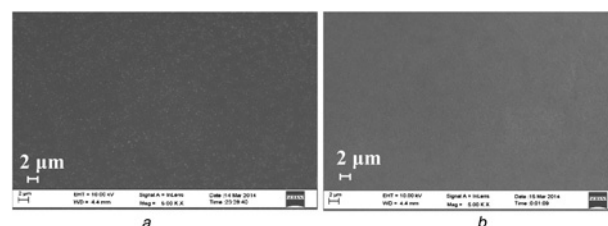


Figure 6 SEM micrographs of the oxide films developed at 8 mA/cm^2 in 4.7 and 6.7 vol% H_2O -added electrolytes
a 4.7 vol%
b 6.7 vol%

be seen from Fig. 7a that the surface is smooth with RMS roughness (R_q) = 0.34 nm and is highly compacted. However, the surface of the oxide deposited in 6.7 vol% H_2O added electrolyte is rough with $R_q = 33.3 \text{ nm}$ and exhibits porosity. The increase in the roughness and porosity could be because of the faster growth rate in electrolytes with increasing water concentration.

3.8. Etch rate study in KOH and TMAH: In wet anisotropic etching, KOH and TMAH were extensively used for the realisation of freestanding structures (e.g. cantilevers, diaphragm) and immovable parts (e.g. cavities, mesa structures) for different applications in the MEMS [22–24]. To explore any material for the structural/masking layer in anisotropic etchants, the study of the etch rate is necessary to investigate the etch selectivity and the etching time for specific etch depths.

The etch rates of the as-grown anodic oxide films were investigated in 25 wt% TMAH and 10 wt% KOH. The etch rates of anodic oxide in 25 wt% TMAH and 10 wt% KOH etchants at three different temperatures (60 , 68 and 76°C) for the films grown in 2.7 vol% water-added electrolyte at 8 mA/cm^2 are presented in Figs. 8a and b, respectively. The oxide grown in

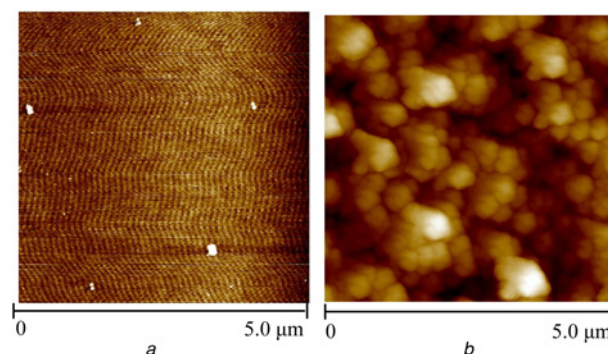


Figure 7 AFM images of the oxide films deposited at 8 mA/cm^2 in 2.7 and 6.7 vol% H_2O -added electrolytes
a 2.7 vol%
b 6.7 vol%

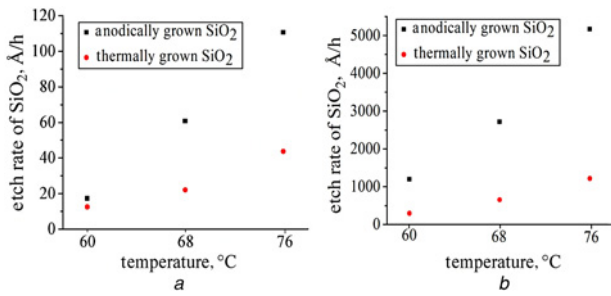


Figure 8 Dependence of oxide etch rate on temperature in 25 wt% TMAH and 10 wt% KOH solutions
 a 25 wt% TMAH
 b 10 wt% KOH

electrolyte containing 2.7 vol% of water was chosen for the etch rate study as this oxide is uniform and denser (non-porous) in comparison to the oxide grown in the electrolytes comprising higher water concentrations. The etch rates of thermal oxide are also included for comparison purpose.

It can be easily noticed from Fig. 8 that the etch rate in TMAH is several times slower than that in KOH. Moreover, the etch rate difference between thermal and anodic oxides decreases with temperature. In the case of TMAH, this difference is lowest at 60°C. Hence, to fabricate the freestanding microstructures using anodic oxide as the structural layer and the cavities using it as the masking layer, anisotropic etching is recommended in TMAH at low temperatures.

3.9. Oxide surface morphology after etching: The quality of the oxide surface after etching in 25 wt% TMAH at different temperatures was examined by an optical microscope. Fig. 9 presents the surface morphology of the oxide samples etched in 25 wt% TMAH solution at 60, 68 and 76°C for 2 h. It can be readily observed that the surfaces appear smooth and pit free except that the film was deposited at a higher etch temperature, that is, 76°C. This implies that anodic oxide can be used as the mask and structural layer for the formation of different types of MEMS structures using 25 wt% TMAH at a low temperature.

3.10. Fabrication of MEMS components: As discussed in the preceding Section, 25 wt% TMAH provides a minimum etch rate for anodic oxides. Another great advantage of 25 wt% TMAH is that it provides a smooth, etched surface morphology [25]. To

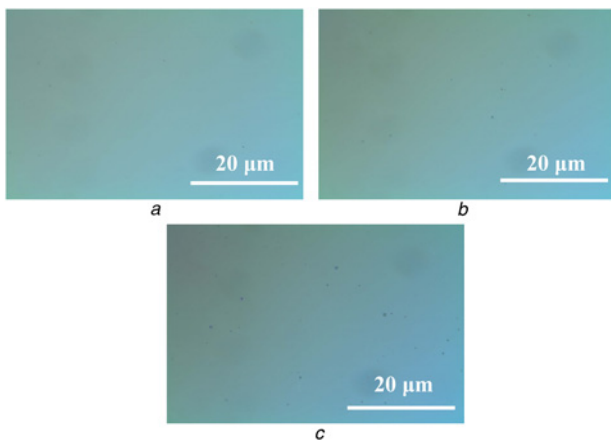


Figure 9 Optical micrographs of the oxide surfaces after etching in 25 wt% TMAH for 2 h at 60, 68 and 76°C
 a 60°C
 b 68°C
 c 76°C

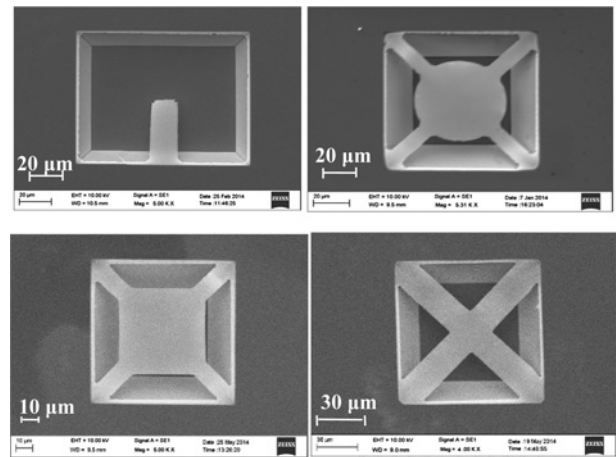


Figure 10 Various shapes of suspended structures of anodic oxide fabricated using 25 wt% TMAH

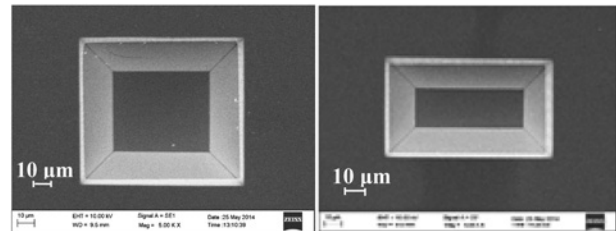


Figure 11 SEM micrographs of the cavities with different shapes in Si{100}, fabricated using anodic SiO₂ as etch mask in 25 wt% TMAH

fabricate freestanding microstructures in this etchant, the as-grown anodic oxide was employed as the structural layer, while for the formation of different shapes cavities it was used as etch mask. To avoid lateral undercutting at the mask edges during the etching process, the mask edges were aligned parallel to the $\langle 110 \rangle$ directions. Fig. 10 shows the SEM images of various shapes of suspended MEMS structures fabricated using as-grown SiO₂ thin film. These types of structures (e.g. cantilever, diaphragm) are widely used for various kinds of sensing applications such as chemical, biological, pressure, acceleration and so on [1, 26–28]. As the Young's modulus of SiO₂ is smaller than Si and Si₃N₄, the oxide-based freestanding structures are useful to enhance the sensitivity of sensors [1].

Fig. 11 presents the SEM micrographs of wet anisotropically etched cavities with different shapes in Si{100} using anodic oxide as the etch mask. The etched depth of the cavity was determined using the 3D measuring laser microscope. Fig. 12 shows the 3D image of a square shape cavity, which was used to

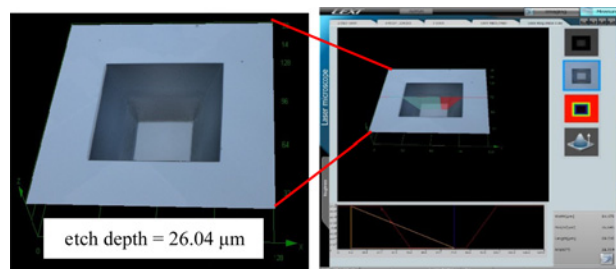


Figure 12 3D view of the square cavity formed in Si{100} using anodic SiO₂ as etch mask in 25 wt% TMAH

measure the etch depth and to observe the top and bottom surfaces. It can be noticed that the top surface protected by the oxide mask and the bottom surface etched by TMAH are smooth, implying that the substrate surface is well protected by the masking (i.e. oxide) layer during the etching process.

4. Conclusion: In the research reported in this Letter, SiO₂ thin films were developed using anodic oxidation of silicon at room temperature. The effect of different parameters on oxide properties has been studied for finding the optimal parameters to explore the oxide films in MEMS. The oxide properties are noticeably affected by the addition of water in the electrolyte. An electrolyte with a low water content provides smooth and uniform films. The refractive index of the as-grown oxides decreases with increasing water content in the electrolyte. In 25 wt% TMAH and 10 wt% KOH, TMAH was found to be most appropriate for the fabrication of MEMS structures using the as-grown anodic SiO₂ as structural and etch mask layers.

5 References

- [1] Peng L., Xinxin L., Guomin Z., *ET AL.*: 'Silicon dioxide microcantilever with piezoresistive element integrated for portable ultrasoluble gaseous detection', *Appl. Phys. Lett.*, 2006, **89**, (7), p. 074104 (3 pages)
- [2] Deal B.E., Grove A.S.: 'General relationship for the thermal oxidation of silicon', *J. Appl. Phys.*, 1965, **36**, (12), pp. 3770–3778
- [3] Hung T.F., Wong H., Cheng Y.C., Pun C.K.: 'New design of anodic oxidation reactor for high-quality gate oxide preparation', *J. Electrochem. Soc.*, 1991, **138**, (12), pp. 3747–3750
- [4] Ju Y.S., Goodson K.E.: 'Process-dependent thermal transport properties of silicon-dioxide films deposited using low-pressure chemical vapor deposition', *J. Appl. Phys.*, 1999, **85**, (10), pp. 7130–7134
- [5] Bhatt V., Chandra S.: 'Silicon dioxide films by RF sputtering for microelectronic and MEMS applications', *J. Micromech. Microeng.*, 2007, **17**, (5), pp. 1066–1077
- [6] Soliman H.M.A., Kashyout A.-H.B.: 'Electrochemical deposition and optimization of thermoelectric nanostructured bismuth telluride thick films', *Engineering*, 2011, **3**, (6), pp. 659–667
- [7] Mende G., Flietner H., Deutscher M.: 'Optimization of anodic silicon oxide films for low temperature passivation of silicon surfaces', *J. Electrochem. Soc.*, 1993, **140**, (1), pp. 182–194
- [8] Duffek E.F., Mylroie C., Benjamini E.A.: 'Electrode reactions and mechanism of silicon anodization in N-methylacetamide', *J. Electrochem. Soc.*, 1964, **111**, (9), pp. 1042–1046
- [9] Pliskin W.A., Lehman H.S.: 'Structural evaluation of silicon oxide films', *J. Electrochem. Soc.*, 1965, **112**, (10), pp. 1013–1019
- [10] Pliskin W.A.: 'Comparison of properties of dielectric films deposited by various methods', *J. Vac. Sci. Technol.*, 1977, **14**, (5), pp. 1064–1081
- [11] Pliskin W.A.: 'Refractive index dispersion of dielectric films used in the semiconductor industry', *J. Electrochem. Soc., Solid-State Sci. Technol.*, 1987, **134**, (11), pp. 2819–2826
- [12] Roschuk T., Wojcik J., Tan X., Davies J.A., Mascher P.: 'Optical and compositional characterization of SiO_xN_y and SiO_x thin films deposited by electron cyclotron resonance plasma enhanced chemical vapor deposition', *J. Vac. Sci. Technol. A*, 2004, **22**, (3), pp. 883–886
- [13] Ceiler Jr. M.F., Kohl P.A., Bidstrup S.A.: 'Plasma-enhanced chemical vapor deposition of silicon dioxide deposited at low temperatures', *J. Electrochem. Soc.*, 1995, **142**, (6), pp. 2067–2071
- [14] Adams A.C., Alexander F.B., Capio C.D., Smith T.E.: 'Characterization of plasma-deposited silicon dioxide', *J. Electrochem. Soc., Solid-State Sci. Technol.*, 1981, **128**, (7), pp. 1545–1551
- [15] Slaoui A., Fogarassy E., Fuchs C., Siffert P.: 'Properties of silicon dioxide films prepared by pulsed-laser ablation', *J. Appl. Phys.*, 1992, **71**, (2), pp. 590–596
- [16] Awazu K., Kawazoe H.: 'Strained Si–O–Si bonds in amorphous SiO₂ materials: a family member of active centers in radio, photo, and chemical responses', *J. Appl. Phys.*, 2003, **94**, (10), pp. 6243–6262
- [17] Grilland A., Neumayer D.A.: 'Structure of low dielectric constant to extreme low dielectric constant SiCOH films: Fourier transform infrared spectroscopy characterization', *J. Appl. Phys.*, 2003, **94**, (10), pp. 6697–6707
- [18] Pai P.G., Chao S.S., Takagi Y., Lucovsky G.: 'Infrared spectroscopic study of SiO_x films produced by plasma enhanced chemical vapor deposition', *J. Vac. Sci. Technol. A*, 1986, **4**, (3), pp. 689–694
- [19] Chou J.S., Lee S.C.: 'Effect of porosity on infrared-absorption spectra of silicon dioxide', *J. Appl. Phys.*, 1994, **77**, (4), pp. 1805–1807
- [20] Babayan S.E., Jeong J.Y., Schutze A., *ET AL.*: 'Deposition of silicon dioxide films with a non-equilibrium atmospheric-pressure plasma jet', *Plasma Sources Sci. Technol.*, 2001, **10**, (4), pp. 573–578
- [21] Schmidt P.F., Owen A.E.: 'Anodic oxide films for device fabrication in silicon. I. The controlled incorporation of phosphorus into anodic oxide films on silicon', *J. Electrochem. Soc.*, 1964, **111**, (6), pp. 682–688
- [22] Pal P., Sato K.: 'Various shapes of silicon freestanding microfluidic channels and microstructures in one step lithography', *J. Micromech. Microeng.*, 2009, **19**, (5), p. 055003 (11 pages)
- [23] Pal P., Sato K.: 'Complex three dimensional structures in Si{100} using wet bulk micromachining', *J. Micromech. Microeng.*, 2009, **19**, (10), p. 105008 (9 pages)
- [24] Zubeil I., Kramkowska M.: 'Possibilities of extension of 3D shapes by bulk micromachining of different Si (h k l) substrates', *J. Micromech. Microeng.*, 2005, **15**, (3), pp. 485–493
- [25] Pal P., Sato K.: 'Fabrication methods based on wet etching process for the realization of silicon MEMS structures with new shapes', *Microsyst. Technol.*, 2010, **16**, (7), pp. 1165–1174
- [26] Rahim R.A., Bais B., Majlis B.Y.: 'Design and analysis of MEMS piezoresistive SiO₂ cantilever-based sensor with stress concentration region for biosensing applications'. Proc. IEEE Int. Conf. on Semiconductor Electronics, ICSE, Malaysia, 2008, pp. 211–215
- [27] Chen Q., Fang J., Ji H.-F., Varahramyan K.: 'Fabrication of SiO₂ microcantilever using isotropic etching with ICP', *IEEE Sens. J.*, 2007, **7**, (12), pp. 1632–1638
- [28] Tang Y., Fang J., Yan X., Ji H.-F.: 'Fabrication and characterization of SiO₂ microcantilever for microsensor application', *Sens. Actuators B*, 2004, **97**, pp. 109–113